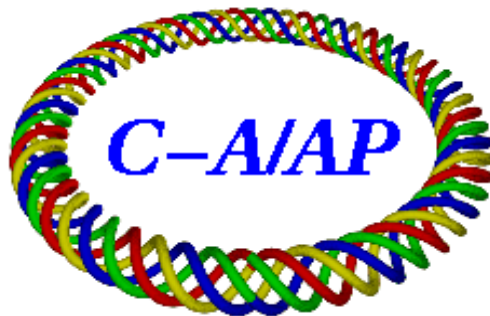


C-A/AP/539

July 2015

**Target and orbit feedback simulations of a
 μ SR beam line at BNL**

**W. W. MacKay, M. Blaskiewicz,
W. Fisher, P. Pile**



**Collider-Accelerator Department
Brookhaven National Laboratory
Upton, NY 11973**

**U.S. Department of Energy
Office of Science, Office of Nuclear Physics**

Notice: This document has been authorized by employees of Brookhaven Science Associates, LLC under Contract No. DE-SC0012704 with the U.S. Department of Energy. The United States Government retains a non-exclusive, paid-up, irrevocable, world-wide license to publish or reproduce the published form of this document, or allow others to do so, for United States Government purposes.

Target and orbit feedback simulations of a μ SR beam line at BNL

W. W. MacKay*

Weirich Consulting, Inc., 25 Rhododendron Cir., Asheville, NC 28805

M. Blaskiewicz, W. Fischer, and P. Pile

BNL, Upton, NY 11972

(Dated: July 28, 2015)

Well-polarized positive surface muons are a tool to measure the magnetic properties of materials since the precession rate of the spin can be determined from the observation of the positron directions when the muons decay. For a dc beam an ideal μ SR flux for surface μ^+ should be about 40 kHz/mm². In this report we show how this flux could be achieved in a beam line using the AGS complex at BNL for a source of protons.

We also determined that an orbit feedback system with a pair of thin silicon position monitors and kickers would miss the desired flux by at least an order of magnitude, even with perfect time resolution and no multiple scattering.

PACS numbers: 29.25.-t, 29.27.Eg, 76.75.+i

I. INTRODUCTION

In this paper, we present improvements of our previous design for a surface muon beam line at BNL[1–3]. We discuss the efficacy of a possible orbit feedback section, as well as an alternate large-bore final focus system to increase the muon density for experiments.

Muon spin rotation, relaxation and resonance (μ SR) is a powerful technique for studying local magnetic fields in samples. When a positive pion decays at rest into a positive muon, the muon has a kinetic energy of 4.119 MeV (momentum 29.792 MeV/c) and its spin is opposite to its direction (negative helicity). If the pion decays near the surface of a target the resulting muons lose little energy, and the result is a beam of muons with a narrow energy distribution and almost 100% polarization. When these positive muons are implanted in matter with a magnetic field the muons precess at a rate proportional to the local field. When the muon decays the positron momentum vector is preferentially aligned with the muon's spin. By measuring the rate of positrons versus time, the precession rate of the muons may be measured thus allowing the magnetic field in the material to be probed.

An ideal μ SR facility[4] would have a flexible energy of 0.5–30 keV for low energy and 4 MeV surface muons with 100% polarization and an energy spread of no more than 5%. Somewhat higher energies could be desirable for penetration through a vacuum vessel. A flux of 40 kHz/mm² would be ideal for a dc beam of surface muons. The spin direction should be transverse to the magnetic field (either external or internal to the sample). For muon microscopy low energy muons should be focused down to an area of $10 \times 10 \mu\text{m}^2$. An ideal pulsed beam would have a repetition rate of around 40 KHz with a pulse width no longer than 26 ns (π^+ lifetime) with as many μ^+ per

pulse as possible over an area of $5 \times 5 \text{ mm}^2$. The pulsed requirements are not achievable with the existing BNL hadron complex.

In this report we examine the possibility of a dc beam of surface muons with a flux of 40 kHz/mm² for a μ SR facility at BNL.

A beam of protons with kinetic energy 1.5 GeV will be extracted from the AGS (see Fig. 1) and focused onto a thin 0.5 mm wide target. An average intensity of 10^{14} proton/s with an rms normalized emittance of $8\pi \mu\text{m}$ is quite achievable from the AGS. Detailed parameters of the AGS and injector chain for μ SR were presented previously.[1, 2]

The tracking code G4BEAMLIN[5] has been used for many simulations of the beam lines in this paper.

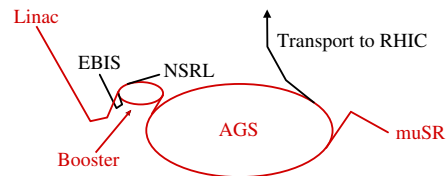


FIG. 1. Schematic of the AGS complex with sections to be used for μ SR shown in red.

II. MUON TARGET AND CAPTURE

Pions which are produced and stop in the target will decay yielding muons which may exit the target if they are within about 0.7 mm of the surface of the graphite target (see Fig. 2). Pions stopped any deeper in the target will produce muons which stop and decay inside the target leading to higher backgrounds and heating of the target and nearby beam-line elements. By making a long, horizontally thin target with the proton beam running down the length and having a waist located at the center of the target, we can maximize surface muons from

* wwmackay@charter.net

pions stopped near the surface with a minimum of background and heating. Fig. 3 shows a 200 mm long, 0.5 mm thick, 50 mm high graphite target with a beam (noninteracting in the figure) having a $\sigma_h^* = 0.25$ mm waist. For 10^{14} protons/s simulations yield about $15 \times 10^9 \mu^+$ /s 0.2 mm from the target's surface. Four times as many positrons are produced, but most are outside the momentum acceptance of the beam line (see Fig. 4).

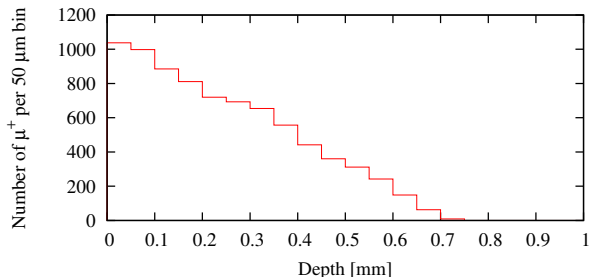


FIG. 2. Number of μ^+ exiting the target from a uniform distribution of 45,000 rest π^+ placed inside a 1 mm thick block of graphite. No μ^+ come from a depth greater than about 0.7 mm. A total of 7933 μ^+ were detected to one side of the graphite block.



FIG. 3. Top view of target and proton beam. The proton beam is focused onto the middle of the narrow graphite $200 \times 50 \times 0.5$ mm³ ($l \times h \times w$) target.

To capture the muon beam, we use a decreasing field from four solenoids placed around the target as shown in Fig. 5. A scan of the capture efficiency versus the field of the upstream solenoid (-1) shown in Fig. 6 demonstrates that capture is more efficient with a negative slope to the axial field around the target. This is reminiscent of Adiabatic Matching Devices[6] used in positron linacs. Fig. 7 shows the momentum distributions of μ^+ and e^+ just downstream of solenoid 3.

We also examined another target geometry equivalent to the source in the MuSIC experiment at the Research Center of Nuclear Physics (RNCP) of Osaka University,

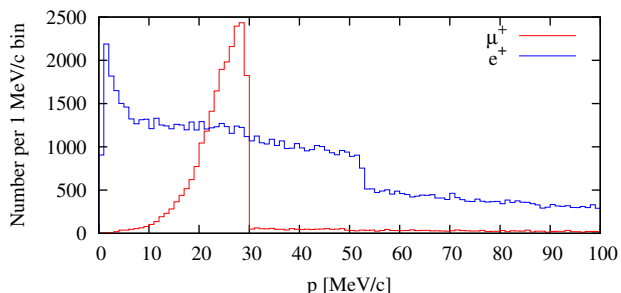


FIG. 4. Momentum distribution of e^+ and μ^+ 0.2 mm from the target's surface from a beam of 1.77×10^8 protons.

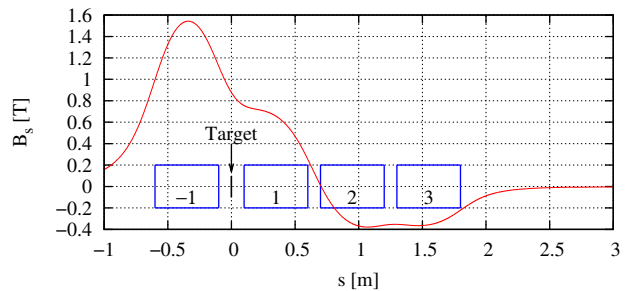


FIG. 5. Layout of target and capture solenoids (blue). The proton beam hits the target placed between two solenoids (-1, 1) as shown with the target and proton beam perpendicular to the solenoid axis. μ^+ are captured by the three solenoids (1, 2, 3) to the right, with the upstream solenoid (-1) adding to the field at the target. The tapered capture fields of the solenoids along the axis are plotted in red. To decouple the magnetized muon beam, we require $\int_0^\infty B_s ds = 0$.

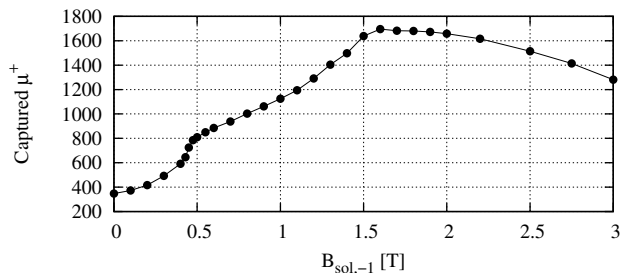


FIG. 6. Fields scan of upstream solenoid (-1).

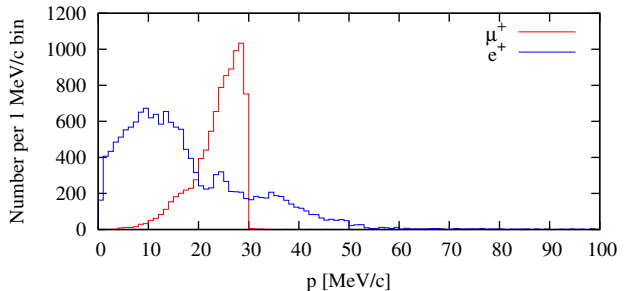


FIG. 7. Momentum distribution of μ^+ and e^+ just after solenoid 3 from a beam of 1.77×10^8 protons.

but found no increase in the rate of surface muons. Details of the comparison with our thin target are given in § V.

Some concerns[7] have been raised about differences in the versions of the Geant4 models when compared to the pion production experiment of Cochran et al.[8] This is not directly addressable for muons coming from pions which have stopped before leaving the target; however comparison of the surface muon momentum distributions shown in Fig. 8 collected from 10^7 protons for three GEANT4 models: BERT, BIC, and ABLA are statistically equivalent with 1490, 1506, 1476 respectively (since $1506 - 1476 = 30 < \sqrt{1476} = 38.4$). For the studies in this paper, we used the QGSP_BERT model.

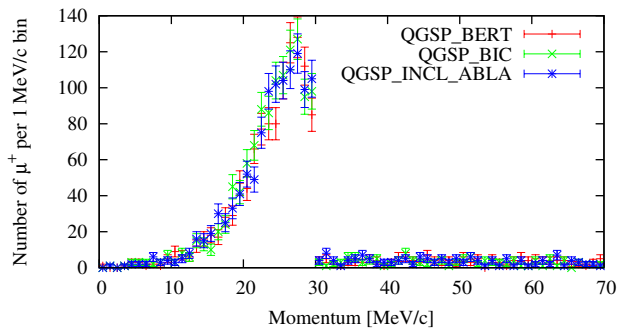


FIG. 8. Surface muon momentum distribution for three different Geant4 models available in G4BEAMLIN-2.14. The versions of the Geant4 physics list simulation engines are QGSP_BERT 3.4, QGSP_BIC 3.4, and QGSP_INCL_ABLA 0.2. A beam of 10^7 protons with kinetic energy 1.5 GeV was run along the target with zero field in the capture solenoids. The detector was placed 0.2 mm away from the surface of the 0.5 mm thick graphite target.

III. DESCRIPTION OF μ SR BEAM LINE

Two versions of a beam line are illustrated in Fig. 9. The first, described in §III A, is a 20 m long line from the target to point A of Fig. 9, and is a simple line with alternating bends to remove neutrals and wrong sign particles and a pair of Wien filters to remove positrons. Results from a variation of the final focus quadrupoles are given in §III A 2.

In order to study the feasibility of feedback for reducing the final spot size of muons at the experiment, the second version is described in §III B and adds two thin silicon foils for position measurements followed by a large arc with horizontal and vertical kicker dipoles to allow feedback for kicking individual muons into a smaller spot size.

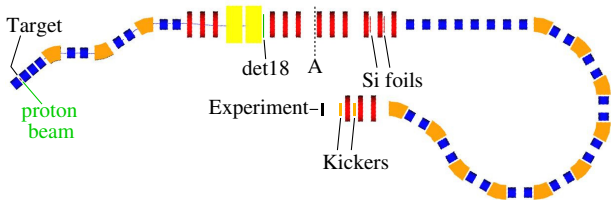


FIG. 9. Layout of beam line in two parts: From left to dashed line A without orbit feedback. The distance from the target to line A is 19.83 m. The extension after the second triplet with the long arc provides delay for orbit feedback from thin Si detectors to steering correctors. The extended beam line has a length of 62.5 m from target to end. Beam line elements are colored as follows: solenoid (blue), dipole (orange), quadrupole (red), separator (yellow). Just downstream of the second separator is the detector “det18” (green).

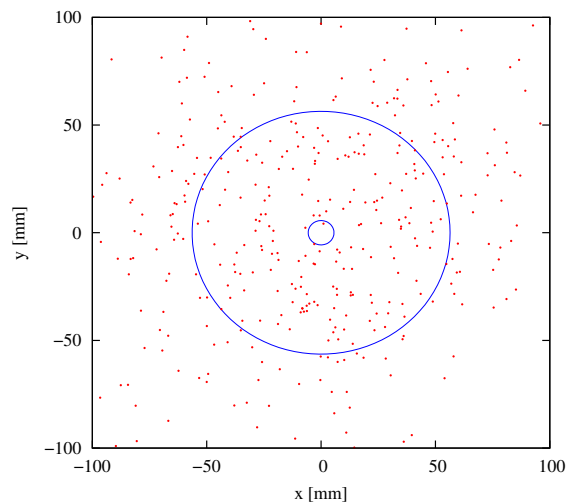


FIG. 10. Transverse distribution of μ^+ at point A from an incident flux of 1.77×10^8 protons on the target. The blue circles enclose areas of 100 cm² and 1 cm².

A. Short μ SR beam line to point A

After capture by the solenoids the surface muons are transported downstream through a series of three sector bend bends. The dipoles remove negative, neutral and off-momentum particles; any remaining pions decay before the end of the beam line. For focusing, we have replaced the earlier quadrupole doublets[1] with solenoid doublets to improve transport and shorten the beam line. Each pair of solenoid doublets are powered in series with opposite polarity to eliminate coupling[2]. Following the first quadrupole triplet are two 1 m long separators (Wien filters) with vertical electric and horizontal magnetic fields to remove any remaining positrons from the muon beam. The separator voltage is 338 kV with a transverse aperture $h \times v$: 600×200 mm² with the magnetic field $B_x = -V_{sep}/hv_{ref}$ where $v_{ref} = 0.256c$ is the velocity of a 28 MeV/c muon. The second quadrupole triplet then can focus the beam onto an experiment station at point A. Parameters of the elements are given in Table I with strengths scaled down from 29.792 to 28.0 MeV/c by a factor of 0.94. Due to an error in a file, the field of dipole D3 was scaled down by an extra factor of 0.94; although this does not appear to have affected the overall results (see § VI).

A flux of 1.77×10^8 protons focused onto the target with $\sigma_h^* = 0.25$ mm and $\sigma_v^* = 1$ mm, produced 171 μ^+ inside a circle of 100 cm² which scales to a rate of 9.7 MHz/cm² for 10^{14} protons/s. Fig. 10 shows the distribution of μ^+ at point A. The location of triplet just upstream of point A is actually too close to the separator for optimum focusing. An improvement of the final focus is discussed below in § III A 2.

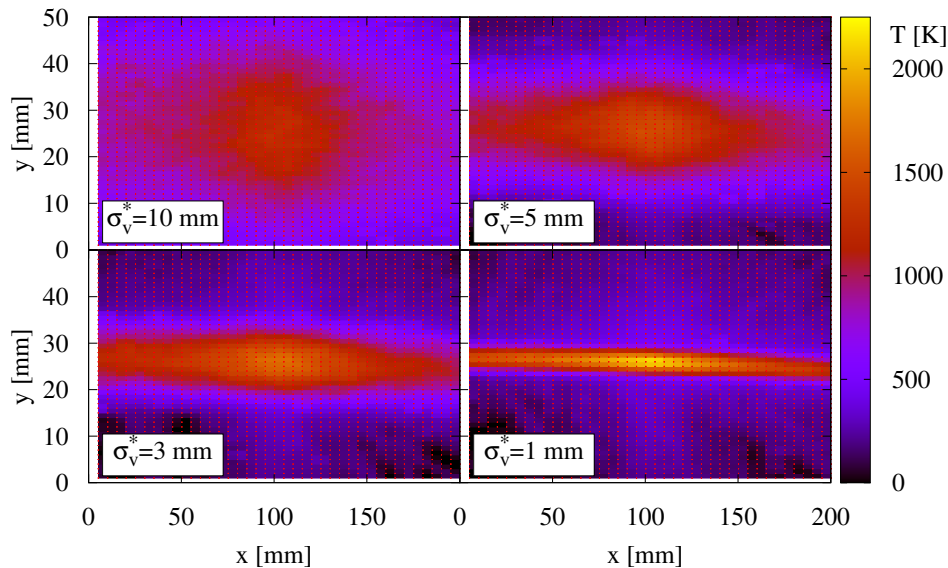


FIG. 11. Heating profiles for a segmented target of 40×50 segments for $\sigma_v^* = 10, 5, 3, 1$ mm. Each simulation used 10^5 protons scaled up to 10^{14} protons/s, and assumed only radiative cooling from both sides of the segment.

TABLE I. Parameters of short beam line to point A.

Element	s_{up}^a [m]	Length [m]	Aperture [m]	Strength ^b [T]
Solenoids			(radius)	[T]
S(-1)	-0.600	0.5	0.24	1.4100
S1	0.100	0.5	0.24	0.5546
S2	0.720	0.5	0.24	-0.3760
S3	1.320	0.5	0.24	-0.3036
SA1	3.420	0.5	0.24	0.2350
SA2	4.219	0.5	0.24	-0.2350
SB1	6.519	0.5	0.24	0.2350
SB2	7.318	0.5	0.24	-0.2350
SC1	9.618	0.5	0.24	0.1701
SC2	10.417	0.5	0.24	-0.1701
Sector bends			($h \times w$)	[T]
D1(-40°)	2.020	1.0472	(0.4 × 0.5)	0.0652
D2(+34°)	5.119	1.0472	(0.4 × 0.5)	-0.0554
D3(-34°)	8.218	1.0472	(0.4 × 0.5)	0.0521 ^c
Quadrupoles			(radius)	[T/m]
Q1a	11.317	0.3	0.4	0.33934
Q1b	12.117	0.3	0.4	-0.40984
Q1c	12.917	0.3	0.4	0.33934
Q2a	16.437	0.3	0.4	0.12020
Q2b	17.237	0.3	0.4	-0.42026
Q2c	18.037	0.3	0.4	0.41106
Separators			($h \times w$)	
V1	13.727	1.0	0.2×0.6	$\left[\begin{array}{l} 338.4 \text{ kV} \\ B_x = -0.0220 \text{ T} \end{array} \right.$
V2	14.927	1.0	0.2×0.6	

^a Distance from target to upstream end of element.

^b Strengths scaled to a muon momentum of 28.0 MeV/c.

^c Due to an error, D3 was scaled down by a factor of 0.94.

1. Vertical size of proton beam and target heating

In our previous report[2], we modeled the proton beam with a vertical waist of 10 mm and then artificially reduced vertical focus to 1 mm of the collected sample of $7536 \mu^+$ from 52.9×10^6 protons incident on the target. This increased the muons at the end of the beam line from 328 with $\sigma_v^* = 10$ mm to 349 with $\sigma_v^* = 1$ mm — slightly larger than a 1- σ increase assuming Poisson statistical errors:

$$\frac{349 - 328}{(328 \times 349)^{1/4}} = 1.14\sigma. \quad (1)$$

Ignoring the errors it corresponds to only a 6% increase in the overall rate of μ^+ .

To model an upper limit to the peak temperature in the graphite target we simulated 10^5 protons on the target for each of several vertical beam waist values. We segmented the 200×50 mm² target into 2000 segments with length \times height = 4.9×0.9 mm² with 0.1 mm gaps between segments. We assumed only radiative cooling from the surfaces of each segment parallel to the x - y plane (not the edges between segments) and used the Stefan-Boltzmann law for black-body radiation

$$P = \epsilon\sigma AT^4, \quad (2)$$

with the Stefan-Boltzmann constant

$$\sigma = 5.6 \times 10^{-8} \text{ Wm}^{-2}\text{K}^{-4},$$

and where $A = 2 \times 4.9 \times 0.9$ mm² is the surface area of the radiating surface, P is the power deposited in the segment by the proton beam, and T is the equilibrium temperature of the segment from balancing the energy deposition against black-body radiation with no conduction or other cooling. We used an emissivity of $\epsilon = 0.8$ for

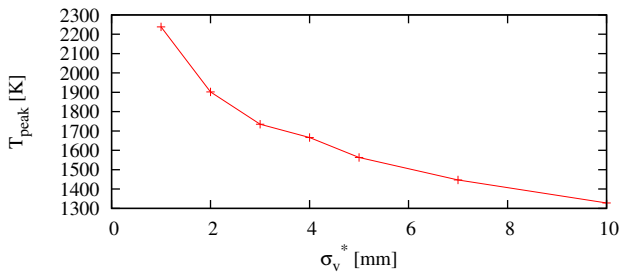


FIG. 12. Peak temperature of target versus σ_v^* assuming only radiative cooling from front and back surfaces and a proton beam flux of 10^{14} protons/s.

TABLE II. Relative μ^+ rates with variation of σ_v^*

σ_v^* [mm]	N_p	R_1^a [GHz]	R_{sep}^b [MHz]	F_{end}^c [kHz/mm ²]
1.0 ^d	177×10^6	14.93	277	9.66 ± 0.74
1.0	100×10^6	14.65	260	7.90 ± 0.89
1.5	100×10^6	14.49	302	8.60 ± 0.93
2.0	100×10^6	14.83	308	10.40 ± 1.02
2.5	100×10^6	14.73	306	9.30 ± 0.96
3.0	100×10^6	14.73	315	9.10 ± 0.95
5.0	100×10^6	14.57	285	8.60 ± 0.93
7.0	100×10^6	14.81	292	8.30 ± 0.91
8.0	100×10^6	14.58	272	8.50 ± 0.92
9.0	100×10^6	14.47	287	8.70 ± 0.93
10.0	99×10^6	14.47	274	7.78 ± 0.89

^a μ^+ rate 0.2 mm from surface of target.

^b μ^+ rate down stream of 2nd separator in det18.

^c μ^+ flux at end of short beam line (point A of Fig. 9).

^d Sample of μ^+ beam from previous run of 177×10^6 protons.

graphite.[9] Profiles of the peak temperature are shown in Fig. 11 for several values of σ_v^* , and the resulting peak temperatures versus vertical beam waist are plotted in Fig. 12.

Scaling back the intensity to decrease target heating (without conduction or cooling) to 1600 K where graphite has a vapor pressure of about 10^{-9} Torr gives 0.33 MHz/cm² for 2.6×10^{13} protons/s, although higher temperatures might be acceptable.[9, 10]

To improve our understanding of the dependence of muon rate with the vertical focus of the proton beam onto the target, we simulated several runs to the end of the beam line at point A with different values of σ_v^* as listed in Table II with rates scaled to 10^{14} protons/s. The flux F_{end} of μ^+ obtained at point A versus σ_v^* is plotted in Fig. 13 and appears to be essentially flat from 1 to 10 mm with an average of 8.76 ± 0.23 kHz/mm². Ideally one would want to retune the beam line for each value of σ_v^* ; however we used the same magnet settings which had been optimized for $\sigma_v^* = 1$ mm throughout the scan. This seems justified since the distribution is quite flat. We can

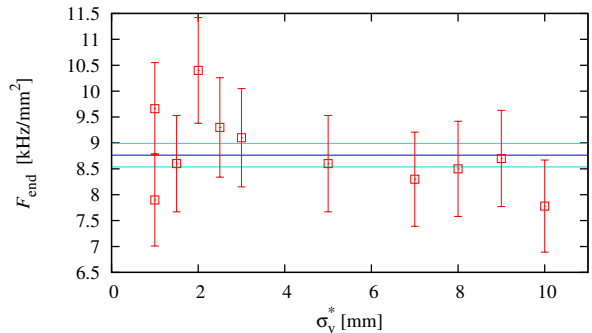


FIG. 13. Flux F_{end} at point A of beam line in Fig. 9 from Table II. The dark blue line indicates the average $\langle \sigma_v^* \rangle = 8.76 \pm 0.23$ kHz/mm² with light blue lines $\pm 1\sigma$ from the average.

conclude that there is no appreciable gain to be made in reducing the vertical waist of the beam, and any value between 5 and 10 mm should not destroy the target.

2. Variation of the final focus at point A

In order to improve the final focus for the short beam line, we added a third triplet downstream of point A as shown in Fig. 14, the idea being to let the beam expand more and then focus it to a smaller spot size (similar to the RHIC interaction regions).

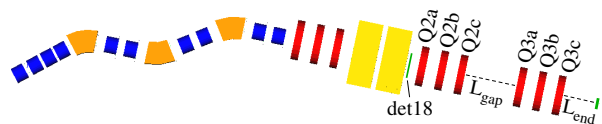


FIG. 14. Modified short μ SR beam line with an extra quadrupole triplet to allow for sharper focus. Detector 18 is shown in green just downstream of the separators.

Using the sample of μ^+ from the $\sigma_v^* = 5$ mm proton beam with a distribution of $287 \mu^+$ in detector 18 at the end of the second separator, we generated a sample of $10,000 \mu^+$ with the same identical 6-d phase-space distribution with the method outlined in § VII, since 287 muons over a wide field was a rather small number to work with for optimizing the final focus down to an area of 1 mm².

A short Python program 2TRIPTUNE.PY was written to speed up tuning the two triplets of the final focus. This program modeled the final focus with simple hard-edged quadrupole and drift matrices. Optimization of the final beam spot was achieved by varying the parameters of the two triplets. For each setting of quadrupoles, the program plotted x - y positions x - x' and y - y' phase space distributions at the entrance of each quadrupole as well as at the end of the line (see Fig. 15). The phase space plots simplified tuning the final focus by hand.

After tuning the quadrupoles and two drift lengths: between Q2c and Q3a, and from Q3c to the end, a solution

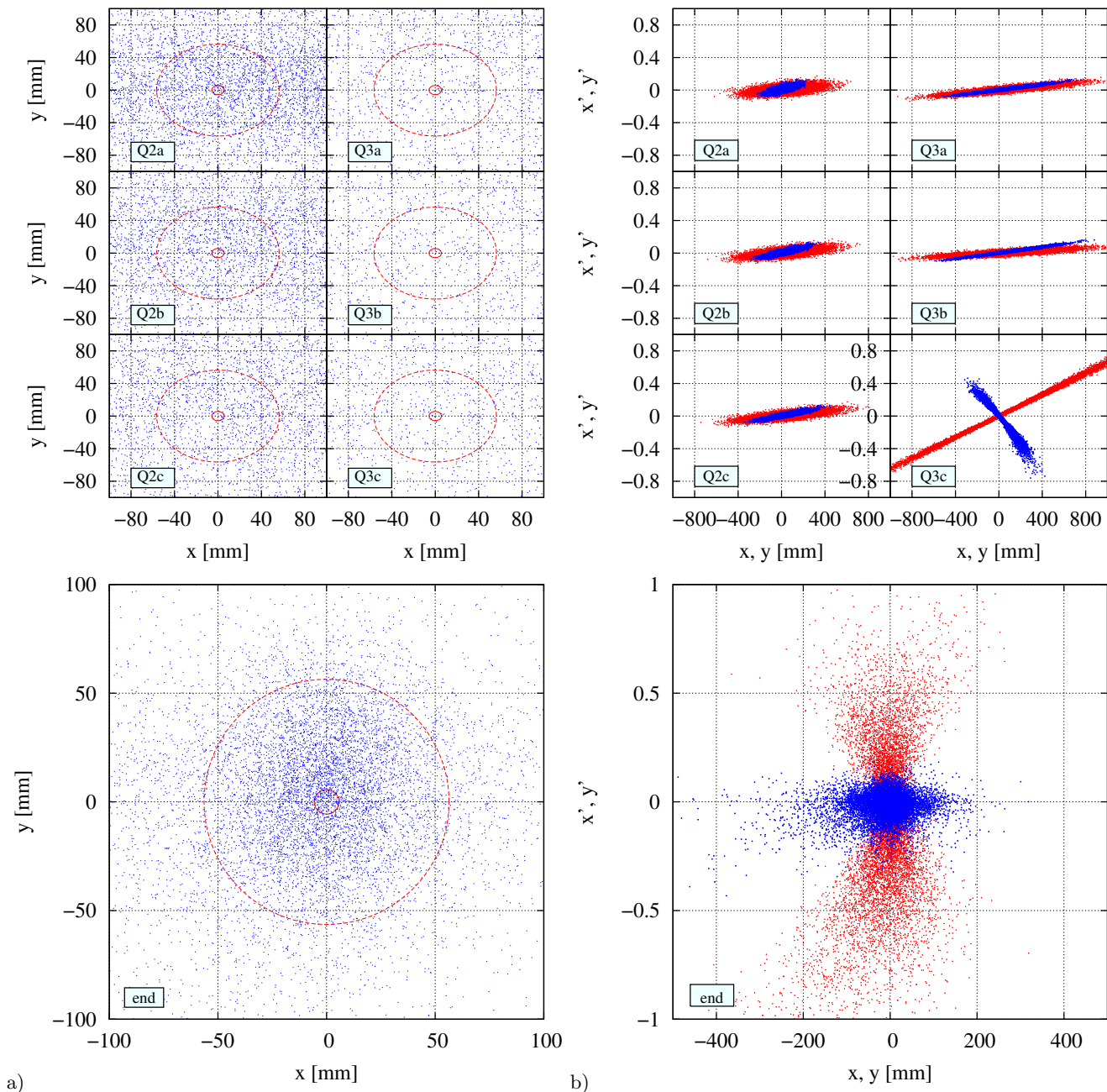


FIG. 15. Position and phase-space plots at the end of the beam line and the entrances of the quadrupoles in the two triplets after the separators. Starting at the end of the 2nd separator, $10,000 \mu^+$ were tracked through the two triplets to the end of the line (point A). a) Positions (x, y) at the entrances of the quadrupoles (top) and end of the line (bottom). The red circles indicate areas of 100 cm^2 and 1 cm^2 . b) Phase-space plots of (x, x') in red and (y, y') in blue at the entrances of the quadrupoles (top) and end of the line (bottom).

was found, with parameters shown in Table IV, having adjustable quadrupole strengths and drift distances between Q2c and Q3a as well as Q3c and the end of the beam line. The parameters where s_{up} is the upstream end of the quadrupole, and gradient strengths shown in the table are for a solution yielding rates shown in Table III and final focus parameters in Table IV. In effect, we only needed to move the second triplet downstream.

Case 1 in Table III using just the 287 muons from the tracking of 10^8 protons with $\sigma_v^* = 5 \text{ mm}$ gave poor statistics with only one μ^+ in a 1 cm^2 circle. Using the generated sample of 10,000 muons (Case 2^b) gave $N_{\text{Scirc}} = 173 \mu^+$ in the 1 cm^2 circle at the end of the beam line. This scales to a flux of $F_{\text{end}} = 49 \text{ kHz/mm}^2$. Fig. 15 shows the position and phase-space plots from 2TRIPTUNE.PY for the full 10,000 muon sample. While this simulation

exceeds the desired flux (40 kHz/mm²), the aperture of the final quadrupoles is quite large, as shown in Fig. 16.

TABLE III. μ^+ rates for the final focus.

Case	N_{det18}	N_{Leirc} 100 cm ²	N_{Scirc} 1 cm ²	F_{end} kHz/mm ²
1	287	194	1	8.7
2 ^a	3000	1848	60	56.6
2 ^b	10000	6125	173	49.0

^a Just the first 3000 μ^+ from generated μ^+ .

^b The full number of generated μ^+ .

TABLE IV. Parameters of Final Focus

Element	s_{up} [m]	Length [m]	Strength [T/m]
Q2a	16.4465	0.3	0
Q2b	17.2465	0.3	0
Q2c	18.0465	0.3	0
Q3a	20.4865	0.3	0.012
Q3b	21.2860	0.3	-0.298
Q3c	22.0855	0.3	0.381
end	23.8855	—	—

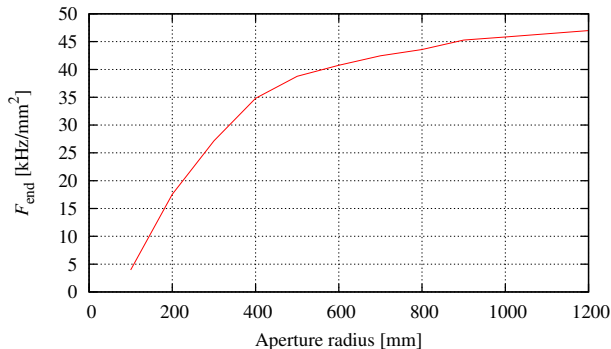


FIG. 16. Flux F_{end} at the end of the beam line versus the aperture of the final focus triplets.

B. Extended beam line for feedback

To study the possibility of orbit feedback, we replaced the experiment at A with the extension (as shown in Fig. 9) consisting of two more quadrupole triplets followed by four solenoid doublets, then five double bend achromats (DBA) and a final triplet for focusing the beam onto an experiment. With the low momentum beam, we can use solenoid doublets to focus between dipoles rather than quadrupoles (see Fig. 17) since

solenoids simultaneously focus the beam in x and y . Two thin silicon foil detectors are placed after the 10th and 11th quadrupoles for position measurements. Two pairs (h and v) pulsed steering kickers are located fore and aft of the last quadrupole for orbit correction. Tables I and V list parameters of elements in these feedback studies.

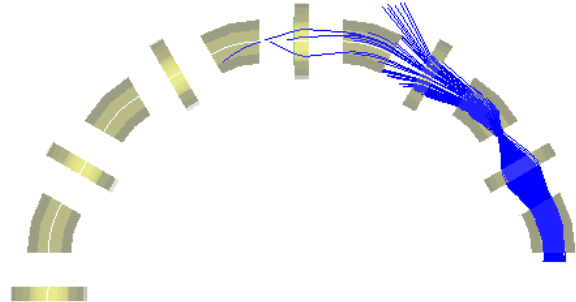


FIG. 17. Using quadrupoles in double bend achromats reduces the dynamic aperture compared to solenoid doublets since a quadrupole must defocus the beam in one plane.

For a parallel 28 MeV/c μ^+ beam incident on a 50 μm thick silicon foil, we may estimate the multiple scattering with the with the formula[11]

$$\theta_{x,\text{rms}} = z \frac{13.6 \text{ MeV}/c}{\beta p} \sqrt{\frac{x}{L_{\text{rad}}}} \left[1 + 0.038 \ln \left(\frac{x}{L_{\text{rad}}} \right) \right] = 31 \text{ mr}, \quad (3)$$

where $L_{\text{rad}} = 9.366 \text{ cm}$, $x = 50 \mu\text{m}$, $p = 28.0 \text{ MeV}/c$, $\beta = 0.25616$, and $z = 1$. The scattering angle $\theta_{y,\text{rms}}$ is identical in the vertical plane. Multiple scattering of μ^+ in a thin silicon foil is shown in Fig. 18 for a relevant range of momenta. For 10,000 μ^+ with initial momentum of 28 MeV/c perpendicularly incident on the foil, Fig. 19 shows the distribution of scattering angles as calculated by G4BEAMLIN. Fig. 20 displays the corresponding distribution of energy losses.

Fig. 21 shows a distribution of time of flight from the first foil and last kicker with a chord distance between foils and kickers of about 6 m. From this we see that

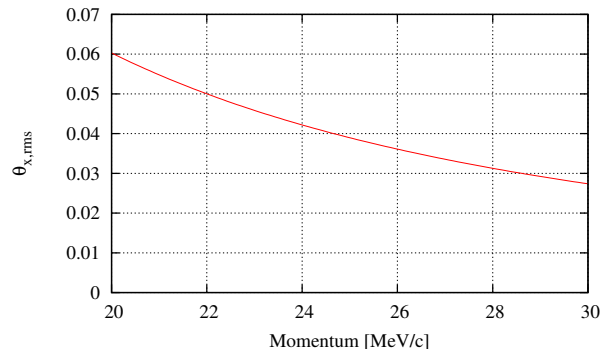


FIG. 18. Multiple scattering angles (from Eq. 3) of μ^+ in a 50 μm foil as a function of momentum.

TABLE V. Parameters of beam line extension for feedback.

Element	s_{up} [m]	Length [m]	Aperture [m]	Strength	Element	s_{up} [m]	Length [m]	Aperture [m]	Strength	
V1	13.727	1.0	$0.1 \times 0.3^{\text{a}}$	169.2 kV $B_x = -0.0220$ T	Quads			(radius)	[T/m]	
V2	14.927	1.0	$0.1 \times 0.3^{\text{a}}$		Q2a	16.437	0.3	0.4	0.3102	
Solenoids					Q2b	17.237	0.3	0.4	-0.4503	
		(radius)		[T]	Q2c	18.037	0.3	0.4	0.3102	
SD1	24.7531	0.5	0.24	0.2254	Q3a	19.337	0.3	0.4	0.2811	
SD2	25.7531	0.5	0.24	-0.2254	Q3b	20.137	0.3	0.4	-0.4004	
SE1	26.7511	0.5	0.24	0.2254	Q3c	20.937	0.3	0.4	0.2811	
SE2	27.7511	0.5	0.24	-0.2254	Q4a	22.237	0.3	0.4	0.3102	
SF1	28.7491	0.5	0.24	0.2254	Q4b	23.046	0.3	0.4	-0.4503	
SF2	29.7491	0.5	0.24	-0.2254	Q4c	23.855	0.3	0.4	0.3102	
SG1	30.7471	0.5	0.24	0.2346	Q5a	59.221	0.3	0.4	0.3624	
SG2	31.7471	0.5	0.24	-0.2346	Q5b	60.021	0.3	0.4	-0.4599	
SH1	33.7943	0.5	0.24	0.2251	Q5c	60.821	0.3	0.4	0.3624	
SH2	34.7943	0.5	0.24	-0.2251	Sector bends				($h \times w$)	[T]
SI1	36.5415	0.5	0.24	0.2251	D4(-30°)	32.6471	1.0472	(0.4 × 0.5)	0.0423	
SI2	37.5415	0.5	0.24	-0.2251	D5(-30°)	35.3943	1.0472	(0.4 × 0.5)	0.0423	
SJ1	39.2887	0.5	0.24	0.2251	D6(-30°)	38.1415	1.0472	(0.4 × 0.5)	0.0423	
SJ2	40.2887	0.5	0.24	-0.2251	D7(-30°)	40.8887	1.0472	(0.4 × 0.5)	0.0423	
SK1	42.0359	0.5	0.24	0.2251	D8(-30°)	43.6359	1.0472	(0.4 × 0.5)	0.0423	
SK2	43.0359	0.5	0.24	-0.2251	D9(-30°)	46.3831	1.0472	(0.4 × 0.5)	0.0423	
SL1	44.7831	0.5	0.24	0.2251	D10(-30°)	49.1303	1.0472	(0.4 × 0.5)	0.0423	
SL2	45.7831	0.5	0.24	-0.2251	D11(-30°)	51.8775	1.0472	(0.4 × 0.5)	0.0423	
SM1	47.5303	0.5	0.24	0.2251	D12(+30°)	54.6247	1.0472	(0.4 × 0.5)	-0.0423	
SM2	48.5303	0.5	0.24	-0.2251	D13(+30°)	57.3719	1.0472	(0.4 × 0.5)	-0.0423	
SN1	50.2775	0.5	0.24	0.2251	Si foils				[μm]	
SN2	51.2775	0.5	0.24	-0.2251	F1	22.639		—	—	
SO1	53.0247	0.5	0.24	0.2251	F2	23.448		—	—	
SO2	54.0247	0.5	0.24	-0.2251	Kickers				[m]	
SP1	55.7719	0.5	0.24	0.2251	K1	60.571	0	—	—	
SP2	56.7719	0.5	0.24	-0.2251	K2	61.171	0	—	—	

^a Reduced aperture.

about 100 ns of flattop is desirable for the kicker pulses leaving a maximum of about 400 ns for signal processing. Since the feedback is to work on single muons, we would want a rate of no more than about 5–7 MHz at the foils.

With the transverse aperture of the separators as given in Table I, 10^{14} protons/s on the target yield 266 MHz at the first foil. By halving the horizontal and vertical separator apertures, we may reduce the required voltage by half and the overall rate at the first foil to about 62 MHz. Fig. 23 shows that the smaller aperture has the additional advantage of reducing the vertical divergence just after the separators by a factor of 0.6 and the horizontal divergence by 0.95. Dropping the proton flux to 10^{13} protons/s then gives a signal rate of 5–6 MHz at the foils which is in the desired range. Even though there is some vertical dispersion introduced by the separator voltage, the reduced aperture did not reduce the

momentum spread of the muon beam.

We ran simulations with monochromatic muon beams at five different momenta to find coefficients of momentum dependent linear transformations for horizontal (x) and vertical (y) kicks at the two locations:

$$\theta_{x,k_2} = A(p)x_{f_1} + B(p)x_{f_2} + D_x(p), \quad (4)$$

$$\theta_{y,k_1} = C(p)y_{f_1}, \quad \text{and} \quad \theta_{y,k_2} = D_y(p), \quad (5)$$

where x_{f_1} , x_{f_2} , and y_{f_1} are the respective horizontal positions at foils 1 and 2 and vertical position at foil 1. Fig. 22 shows how the muon momentum p can be determined from the time of flight between the two foils. Momentum dependent fits to the five parameters are shown in Fig. 24.

Results from autotuning for different foil thicknesses are shown in Fig. 25 and summarized in Table VI with rates scaled to 10^{13} protons/s. Clearly the multiple scat-

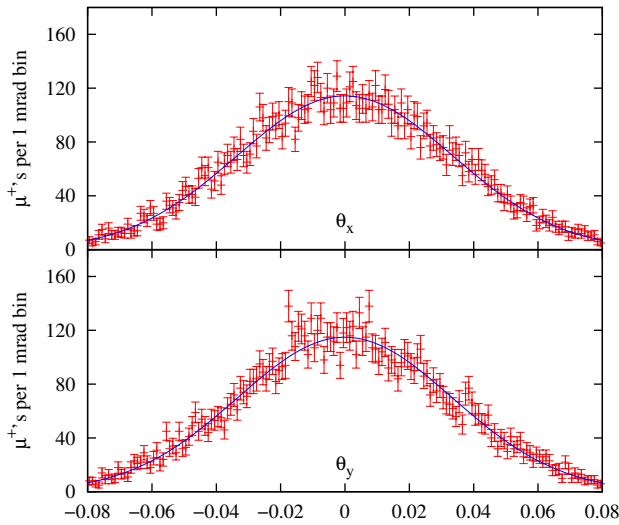


FIG. 19. G4BEAMLIN simulation of multiple scattering angles for 10^4 parallel μ^+ with 28.0 MeV/c incident on a 50 μm thick silicon foil. Blue curves are Gaussian fits. Top: distribution of horizontal scattering angles with a fitted Gaussian having $\sigma = 34$ mr; Bottom: vertical distribution with $\sigma = 33$ mr.

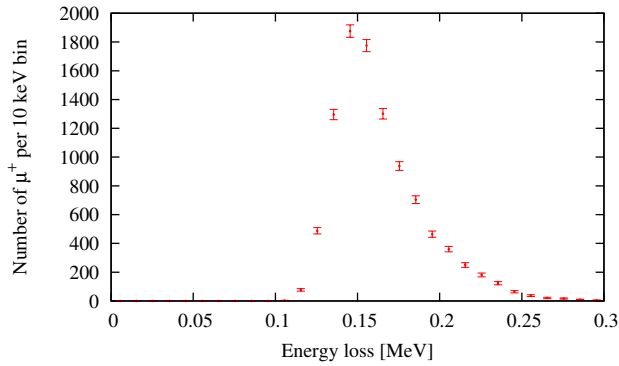


FIG. 20. Simulated energy loss of 28 MeV/c μ^+ passing through 50 μm of silicon.

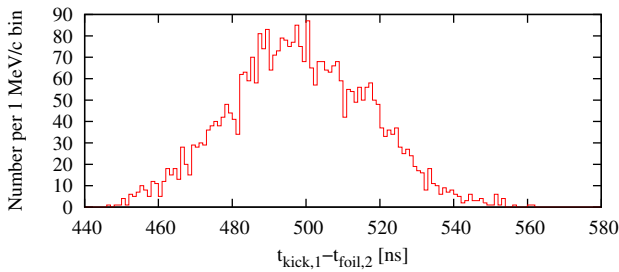


FIG. 21. Distribution of muon time of flight from first foil to last kicker. The longest straight-line distance from foil to kicker is 6 m which corresponds to 30 ns for a 0.66 c cable.

tering in foils thicker than 10 μm will wash out orbit feedback. At best, with zero-thickness foils having perfect time resolution we could only expect about 5 kHz/mm²

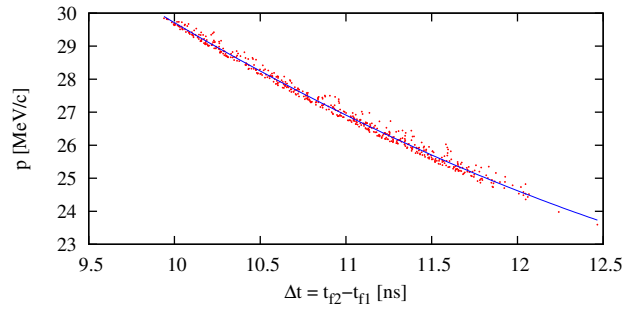


FIG. 22. Momentum versus time of flight between the two foils. The blue curve is a parabolic fit to the data.

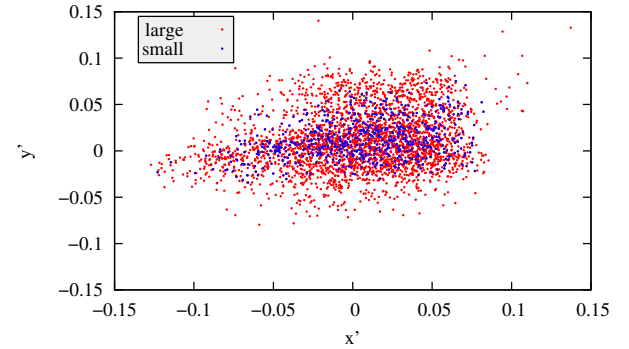


FIG. 23. Halving the aperture of the separators reduces the vertical divergence a factor of 0.6 and the horizontal divergence slightly by a factor of 0.95 .

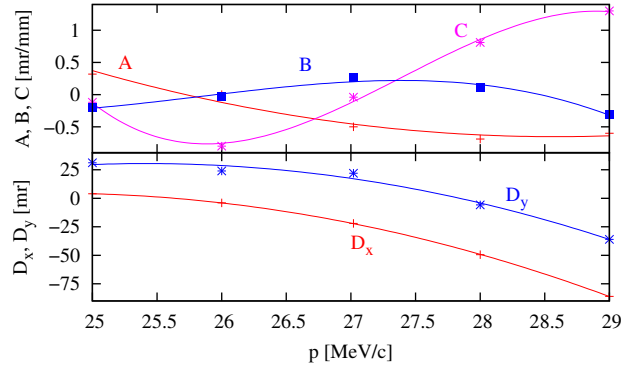


FIG. 24. Fits to autotuning coefficients from tuning of monochromatic muon beams. A , D_x , and D_y are parabolic fits, and B and C are cubic fits.

which is less than the 8.76 kHz/mm² rate in Fig. 13. Adding realistic jitter in the time measurement[12] could reduce the achievable flux even more.

1. Effect of multiple scattering on perfect correction.

In order to demonstrate the effect of multiple scattering on our correction, we use a simple idealized correction scheme with single horizontal and vertical correctors lo-

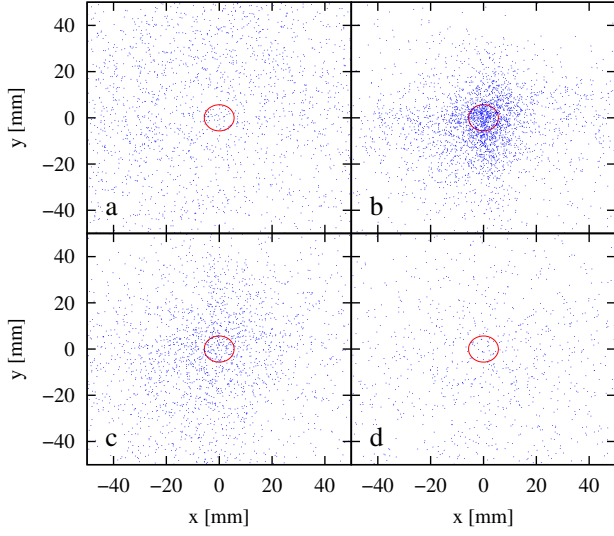


FIG. 25. Muon distribution a) with no foils or autotuning, b) with autotuning and zero thickness foils, c) with 10 μm foils and autotuning, d) with 50 μm foils and autotuning. The red circles have an area of 1 cm^2 .

TABLE VI. μ^+ Rates with Autotuning.

Thickness μm	Number of μ^+ ^a in 1 cm^2	Rate ^b kHz/ mm^2	Autotuning
0	39	0.50	no
0	409	5.27	yes
10	94	1.21	yes
50	26	0.33	yes

^a from 5000 μ^+ at end of 2nd separator.

^b scaled to 10^{13} protons/s.

cated at a kicker plane a distance $L = 1.35$ m upstream of the focal plane as indicated in Fig. 26. In the horizontal plane, we model an ideal correction for a muon arriving at the plane of the kicker at position x with slope

$$\theta_1 = \tan^{-1}(p_x/p_z), \quad (6)$$

to focus onto a single point of the focal plane by applying a kick $\Delta\theta = \theta_2 - \theta_1$ where

$$\theta_2 = \tan^{-1}(x/L). \quad (7)$$

The vertical kick is calculated in the same manner.

Fig. 27 shows that a monochromatic sample of 10,000 μ^+ were tracked from det18 just after the separators to the kicker plane (the 2nd kicker location after the last quadrupole in Fig. 9) and then corrected to a single point.

There are three separate effects which come into play with the insertion of foils into the beam line:

1. average energy loss of the beam as demonstrated by the momentum shifts in Fig. 28;
2. momentum spreading also seen in Fig. 28;

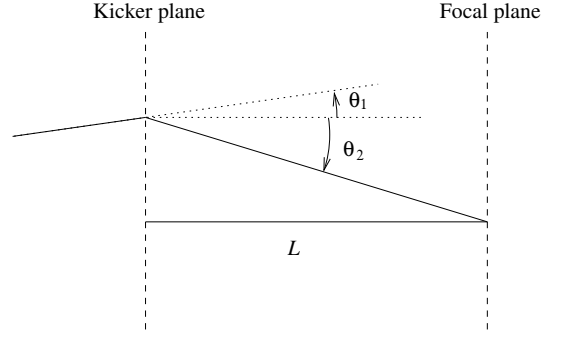


FIG. 26. For an ideal correction a muon entering from the left should be kicked by an angle $\Delta\theta = \theta_2 - \theta_1$ onto a single point in the focal plane.

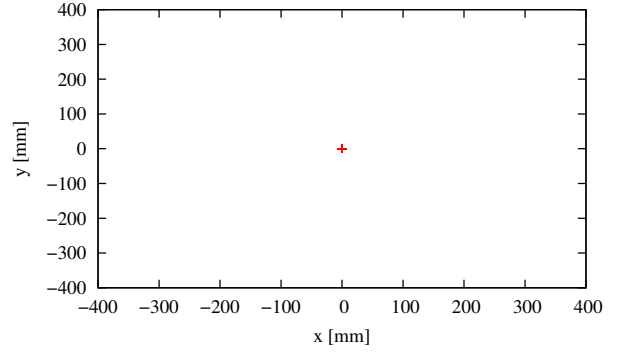


FIG. 27. Correction with no multiple scattering or energy loss from foils. Of 10,000 μ^+ tracked from det18, 3173 survived to the end of the line and were corrected to a single point.

3. angular spreading as plotted in Fig. 19.

To adjust for the average energy loss, we typically scale all the fields of magnets downstream of the foil by a factor $f_{sc,1}$. Fig. 29 shows how the corrected trajectories smear out from the single point of Fig. 27 when $f_{sc,1} = 0.9786$ corresponding to the expected momentum shift from a single 50 μm foil. Figs. 30 and 31 show how the

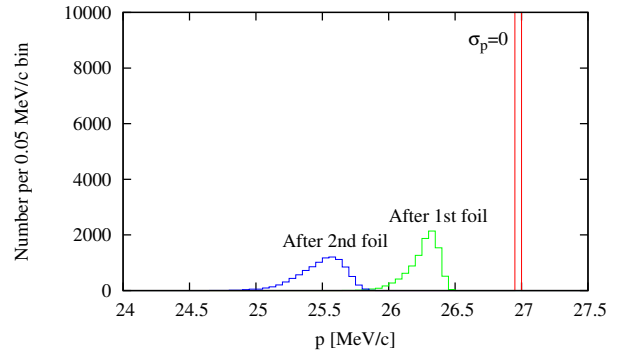


FIG. 28. Momentum spreading of a monochromatic muon beam from two 50 μm silicon foils.

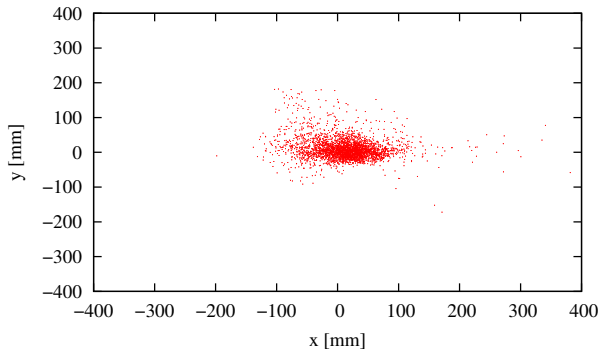


FIG. 29. Effect of scaling the fields downstream of the first foil location by a factor of $f_{sc,1} = 0.9786$. The foils were not inserted for this simulation, so the beam remains monochromatic without multiple scattering.

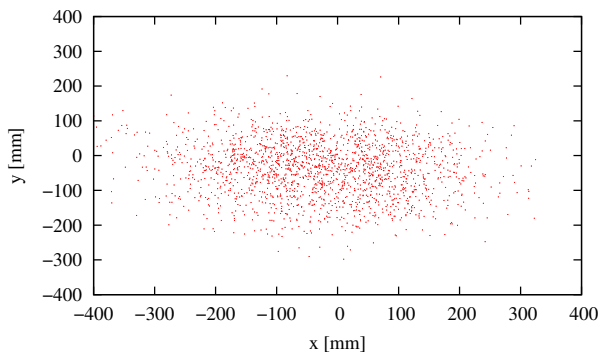


FIG. 30. Smearing from 50 μm foils with $f_{sc,1} = 1$. This is predominantly from angular scattering but has the effect of momentum smearing as well.

single spot smears out with foils of 50 μm and 10 μm respectively.

We should also note that the solenoids are nonlinear elements with large fringe fields. In fact all of the elements must be considered to be nonlinear, since the momentum spread is quite large for the actual beam as can be seen in Fig. 22.

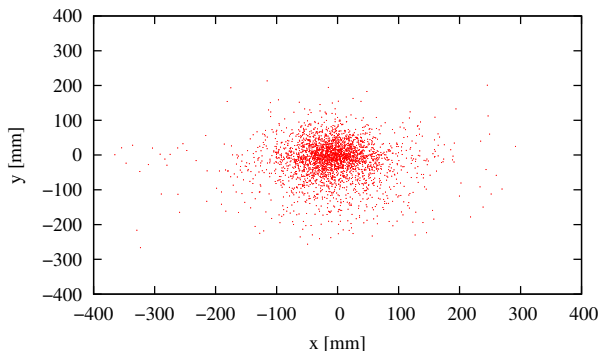


FIG. 31. Smearing from 10 μm foils with $f_{sc,1} = 1$.

TABLE VII. Production from 10^8 protons

Kinetic energy	μ^+	e^+	π^+
392 MeV	14286	150029	28272
1500 MeV	318872	1016798	1030494

IV. CONCLUSIONS

A 1.5 GeV kinetic energy proton beam focused with a $\sigma_h^* = 0.25$ mm horizontal waist onto the center of a 200 mm long, 50 mm high, 0.5 mm wide graphite target can produce a large number of surface muons since muons from stopped pions can only exit the target from no deeper than about 0.7 mm. For a flux of 10^{14} protons/s, we expect about $15 \times 10^9 \mu^+$ with $p < 30$ MeV/c at 0.2 mm from the surface of the target and a flux of about around 35 kHz/mm² at the end of a 20 m long beam line depending on the target cooling. With larger aperture quadrupoles for the final focus, it appears that might be possible to achieve or even exceed the desired 40 kHz/mm² flux.

We also investigated the feasibility of single-particle orbit feedback with a large U-shaped turnaround to allow for signal processing from a pair of thin silicon foils for position measurements to pulsed steering magnets. An algorithm for increasing the final density of muons works in principle with zero-thickness foils to measure position and momentum via time-of-flight. Multiple scattering from foils of around 10 μm can decrease or even eliminate any gain in density at an experiment. However the additional requirement of position measurements with steering corrections for individual muons limits the muon rate at the position detectors to 5–7 MHz. Even for zero-length foils with perfect time resolution, this limits the flux to an order of magnitude below the desired value of 40 kHz/mm².

V. APPENDIX: STUDY OF MUSIC TARGET

We decided to investigate whether muon production on a larger target placed inside a solenoid might produce a high flux in the direction opposite to the incident proton beam as is done by the MuSIC beam line at the Research Centre for Nuclear Physics (RCNP) in Osaka.[13, 14] To do this, we made an approximate model of the MuSIC target and capture solenoid with G4BEAMLIN using Fig 1. of Ref. 14. The MuSIC target is a 20 cm long solid graphite target with a radius of 1 cm and is placed inside a superconducting 3.5 T solenoid of about 1.65 m length with an inner radius of 0.375 m. A stainless steel absorber is inserted inside the magnet. Fig. 32 shows the G4BEAMLIN model approximating the MuSIC target and solenoid with the target axis at 22° to the axis of the solenoid.

Fig. 33 shows the momentum distribution of μ^+ in

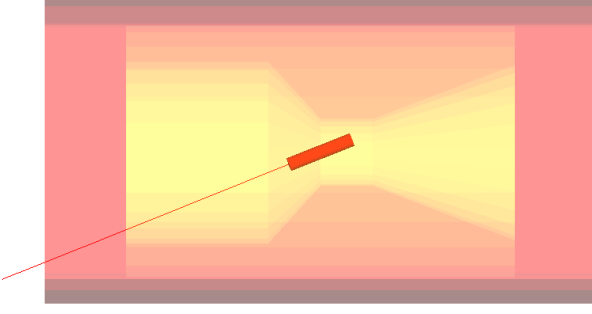


FIG. 32. Approximate model of the MuSIC target and capture solenoid. The proton beam (in red) enters from the lower left and hits the graphite target. A stainless steel absorber with a grail-shaped cutout is inserted into the solenoid to shield the coils from background. The muons are collected to the left in the backscattered direction.

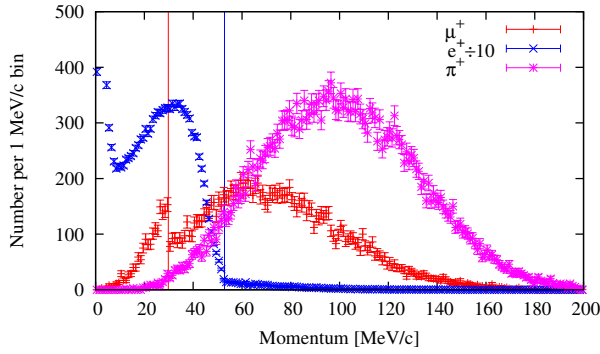


FIG. 33. Momentum distribution of μ^+ , e^+ (divided by 10) and π^+ from 10^8 protons with kinetic energy 392 MeV. Only about 11% of the μ^+ are surface muons (with $p < 30$ MeV/c). The red vertical line is at the maximum momentum of a μ^+ from the decay of a stopped pion. The blue vertical line is at the maximum momentum of a e^+ from the decay of a stopped muon. Only about 11% of the μ^+ are surface muons (with $p < 30$ MeV/c).

the backward direction for protons with kinetic energy (392 MeV) of the MuSIC experiment[14]. Only about 11% of these muons have less than 30 MeV/c. A similar plot for the BNL kinetic energy (1.5 GeV) in Fig. 34 shows that only 4.6% of the muons are surface muons with $p < 30$ MeV/c. Table VII shows the numbers of μ^+ , e^+ , and π^+ collected in the back-scattered direction for both 392 MeV and 1.5 GeV protons.

Measurements [14] of the MuSIC muon source gave about $3 \times 10^8 \mu^+$ with a $1 \mu\text{A}$ beam. This corresponds to a yield for surface μ^+ of around

$$\frac{3 \times 10^8 \mu^+/\text{s}}{6 \times 10^{12} \text{ protons/s}} \times 11\% = 5.5 \times 10^{-6} \mu^+/\text{proton}.$$

Scaling up to 1.5 GeV gives

$$5.5 \times 10^{-6} \times \frac{318872 \times 4.6\%}{14286 \times 11\%} = 5.1 \times 10^{-5} \mu^+/\text{proton}.$$

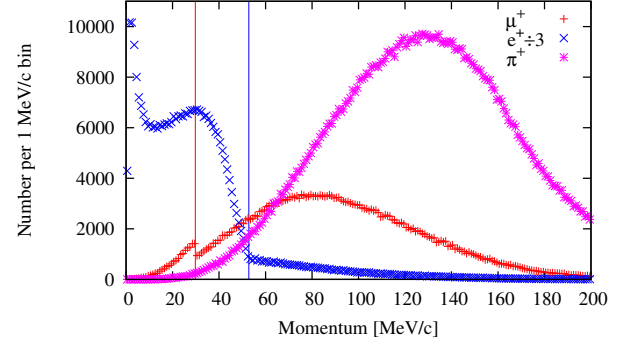


FIG. 34. Momentum distribution of μ^+ , e^+ (divided by 3) and π^+ from 10^8 protons with kinetic energy 1.5 GeV. The red vertical line is at the maximum momentum of a μ^+ from the decay of a stopped pion. The blue vertical line is at the maximum momentum of a e^+ from the decay of a stopped muon. Only about 4.6% of the μ^+ are surface muons (with $p < 30$ MeV/c).

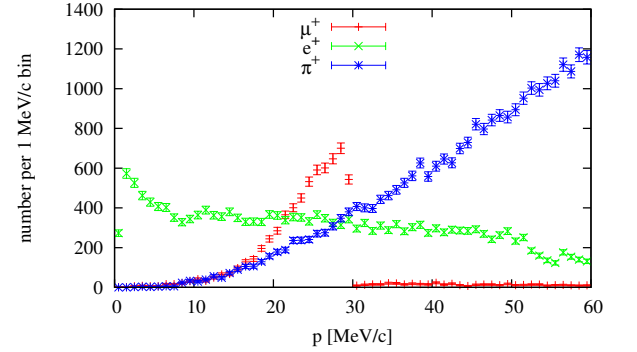


FIG. 35. Momentum distributions of μ^+ , e^+ , and π^+ 0.2 mm away from the surface of the 0.5 mm thick graphite discussed in § II with a beam of 52.879×10^6 protons.[2]

This is equivalent to what we obtained in Ref. 2 at the end of the capture solenoids

$$\frac{2696 \mu^+}{53 \times 10^6 \text{ proton}} = 5.1 \times 10^{-5} \mu^+/\text{proton}.$$

While the numbers of surface muons per proton are equivalent for the MuSIC target and the 0.5 mm thick target of § II, comparison of Figs. 34 and 35 demonstrates that the backgrounds are much smaller for the thin target shown in Fig. 3. If muons of momentum higher than 30 MeV/c are desired then a thicker target with a different incident angle of the beam would be required.

VI. APPENDIX: EFFECT OF LOW FIELD IN D3

The original beam line was set up with a reference momentum of 29.792 MeV/c, i. e. the momentum of the μ^+ from the two-body decay of a π^+ at rest. The momentum distribution of surface muons tails off toward

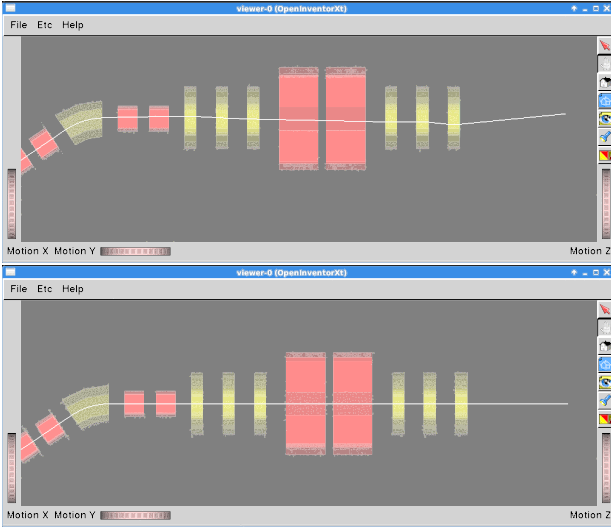


FIG. 36. The top figure shows a reference trajectory (28 MeV/c) with the field of D3 too low by a factor of 0.94 ($Bd3=0.052088$ T). The bottom figure shows the reference trajectory with correct field of $Bd3=0.055413$ T.

lower momenta as shown in Fig. 7. We found that scaling all the fields of the beam line downward by a factor $f_{scal}=0.94$ (corresponding to a design momentum of 28 MeV/c) peaked the number of muons accepted by the beam line[2].

The code in the G4BEAMLIN scripts contained three lines for setting the fields of the first three dipoles as follows:

$$\text{param -unset Bd1}=0.06937*\$f_{scal} \quad (8)$$

$$\text{param -unset Bd2}=-0.05895*\$f_{scal} \quad (9)$$

$$\text{param -unset Bd3}=-\$Bd2*\$f_{scal} \quad (10)$$

Clearly in Eq. 10 the value $Bd3$ is scaled once too often. This error appears to have been introduced in the upstream model back in May, 2013, and was only noticed twenty four months later. Fig. 36 shows how a reference trajectory is affected by this 6% drop in the field of D3.

TABLE VIII. Comparison of μ^+ survival with D3 field.

Model	s [m]	D3 low	D3 OK
Short (to A)	15.947 ^a	491	476
	19.838 ^b	171	161
Extended ^c	15.947 ^a	114	101
	61.521 ^b	10	11

^a det18 just after 2nd separator

^b 100 cm² detector

^c With reduced separator aperture.

The survival of muons is plotted in Fig. 37 for for the last 10 m of the short beam line, and Table VIII shows

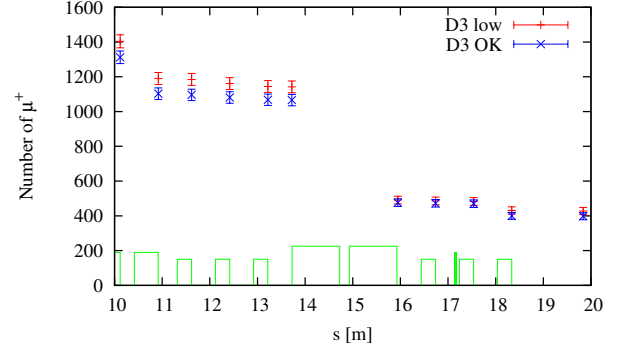


FIG. 37. Comparison of μ^+ survival in the last 10 m of the short beam line up to point A, using the sample of μ^+ from 177×10^6 protons on the target. Interestingly, the low field seems to do slightly better.

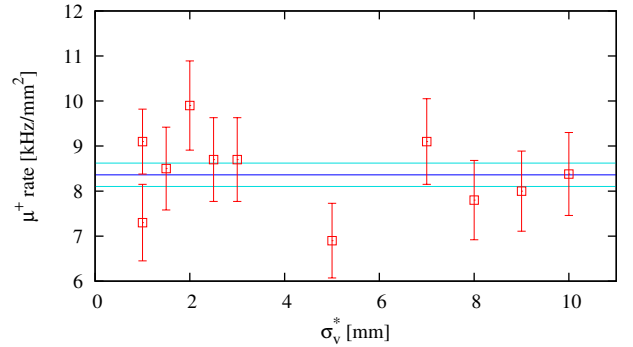


FIG. 38. Revised version of Fig. 13 with the D3 field raised to 0.05541 T. The dark blue line again indicates the average $\langle \sigma_v^* \rangle = 8.36 \pm 0.26$ kHz/mm² with light blue lines at $\pm 1\sigma$ from the average. This average is slightly lower than the 8.76 ± 0.23 of Fig. 13.

the number of μ^+ just after the separator and at the end of the beam line for the short and extended models. The numbers with the low field values are slightly better, but are not very different. With the field of D3 raised to the nominal value of 0.05541 T, Fig. 38 shows a revised version of Fig. 13 with a slightly lower average value. The magnet strengths were optimized with the lower value, so that might explain a slight increase given that the magnet apertures are quite large.

Table IX gives revised strengths for the three triplets with the D3 at its correct strength. By combining the μ^+ samples from 11 runs of 1.176×10^9 protons listed in Table II we have 189,108 μ^+ at 0.2 mm from the surface of the target. Tracking these through the beam line using G4BEAMLIN with the corrected D3 strength and the optimized quadrupole strengths in Table IX gives 39 μ^+ in a 1 cm² circle. This corresponds to

$$\frac{1 \times 10^{14} \text{ protons/s}}{1.176 \times 10^9 \text{ protons}} \times 39 \mu^+ = 33 \text{ kHz/mm}^2. \quad (11)$$

Using an aperture radius of 0.4 m, the program 2TRIP-

TABLE IX. Revised Parameters of Final Focus

Element	s_{up} [m]	Length [m]	Strength ^a [T/m]
Q1a ^b	11.3170	0.3	0.336
Q1b ^b	12.1170	0.3	-0.418
Q1c ^b	12.9170	0.3	0.336
Q2a	16.4465	0.3	0.059
Q2b	17.2465	0.3	-0.060
Q2c	18.0465	0.3	0.041
Q3a	20.4865	0.3	0.009
Q3b	21.2860	0.3	-0.298
Q3c	22.0855	0.3	0.392
end	23.8855	—	—

^a After optimizing for the correct D3 field of 0.05541 T.

^b Reoptimized 1st triplet upstream of separators.

TUNE.PY got $44 \mu^+$ in a 1 cm^2 circle which corresponds to 37 kHz/mm^2 after correcting for muon decays in the last 3.9 m of the beam line. This is fairly good agreement considering the differences in the track integration of G4BEAMLIN compared with simple hard edge matrices, and both are close to the value 35 kHz/mm^2 in Fig. 16.

VII. APPENDIX: GAUSSIAN 6-D PHASE SPACE GENERATOR

We use the 6-d phase-space vector

$$\mathbf{X} = \begin{pmatrix} x \\ p_x \\ y \\ p_y \\ t \\ p_z \end{pmatrix} \quad (12)$$

for a single particle with time t rather than z , since for a given detector in G4BEAMLIN z is a constant, but the arrival time t varies from particle to particle. (In principle, one might want to multiply t by the speed of light or particle's velocity; however this is unnecessary since our algorithm preserves units.)

Given a distribution of N particles, we may calculate the average

$$\langle \mathbf{X} \rangle = \frac{1}{N} \sum_{i=1}^N \mathbf{X}_i, \quad (13)$$

and the covariance matrix

$$\boldsymbol{\Sigma} = \frac{1}{N} \sum_{i=1}^N (\mathbf{X}_i - \langle \mathbf{X} \rangle) (\mathbf{X}_i - \langle \mathbf{X} \rangle)^T \quad (14)$$

$$= \frac{1}{N} \sum_{i=1}^N \mathbf{X}_i \mathbf{X}_i^T - \langle \mathbf{X} \rangle \langle \mathbf{X} \rangle^T \quad (15)$$

The inverse of the $\boldsymbol{\Sigma}$ matrix is called the Fisher matrix

$$\boldsymbol{\Xi} = \boldsymbol{\Sigma}^{-1}, \quad (16)$$

and the Gaussian distribution function may be written as

$$\frac{dN}{dx dp_x dy dp_y dt dp_z} = \frac{N}{(2\pi)^3 \epsilon_x \epsilon_y \epsilon_z} e^{\frac{1}{2} \mathbf{X}^T \boldsymbol{\Xi} \mathbf{X}}. \quad (17)$$

The Fisher matrix is symmetric, so we may use an SO(6) rotation matrix \mathbf{R} to diagonalize it

$$\mathbf{D} = \mathbf{R} \boldsymbol{\Xi} \mathbf{R}^T, \quad \text{or} \quad (18)$$

$$\boldsymbol{\Xi} = \mathbf{R}^T \mathbf{D} \mathbf{R}. \quad (19)$$

The argument of the exponential in Eq. 17 then becomes

$$-\frac{1}{2} \mathbf{X}^T \boldsymbol{\Xi} \mathbf{X} = -\frac{1}{2} (\mathbf{X}^T \mathbf{R}^T) \mathbf{D} (\mathbf{R} \mathbf{X}) \quad (20)$$

$$= -\frac{1}{2} \sum_{j=1}^6 D_{jj} V_j^2, \quad (21)$$

where the vector $\mathbf{V} = \mathbf{R} \mathbf{X}$. The six coordinates of \mathbf{V} may be generated in pairs using a simple 2-d Gaussian generator since the off-diagonal elements of \mathbf{D} are zero.

To obtain a 2-d Gaussian distribution, we use a flat pseudo-random number generator with a range $[0, 1)$. For example, to generate (V_1, V_2) for a particle from a pair of random numbers ξ_1 and ξ_2 , we first calculate the polar coordinates

$$r = \sqrt{-2 \log(1 - \xi_1)}, \quad \text{and} \quad \theta = 2\pi \xi_2, \quad (22)$$

and then

$$V_1 = \frac{r}{\sqrt{D_{11}}} \cos \theta, \quad \text{and} \quad V_2 = \frac{r}{\sqrt{D_{22}}} \sin \theta. \quad (23)$$

Similarly, we generate the pairs (V_3, V_4) and (V_5, V_6) from four more random numbers. Finally we must invert the rotation

$$\mathbf{X} = \mathbf{R}^T \mathbf{V}, \quad (24)$$

to get back to the original coordinate system.

As an example, tracking muons from the target down to the end of the 2nd separator, gave 287 in detector det18. Then 10,000 μ^+ were generated to match the phase space distribution of the original 287 muons. Comparison phase-space projections are shown in Fig. 39, and

phase space correlations are plotted in Fig. 40. The negative slope indicating vertical dispersion in the y' - p plot of Fig. 40 comes from the electric field of the separators. The angular momentum $L_z = xp_y - yp_x$ versus momentum plot is nicely symmetric for both distributions. If there had still been solenoidal coupling in the tracked

distribution, then the two distributions would not match in the L_z plot, since this 6-d generator does not work for a magnetized beam. In the case of solenoidal fields, perhaps replacing the kinetic momenta \vec{p} by canonical momenta $\vec{P} = \vec{p} + q\vec{A}$ where $q\vec{A}$ is charge times an appropriate vector potential for the magnetic field might produce a reasonable distribution for a magnetized beam.

-
- [1] M. Blaskiewicz *et al.*, in *Proceedings of IPAC2013* (2013) p. 3749.
 - [2] W. W. MacKay *et al.*, *μ SR Beam Line Design Studies*, Tech. Rep. C-A/AP/501, BNL-103717-2013-IR (BNL, 2013).
 - [3] W. W. MacKay, M. Blaskiewicz, W. Fischer, and P. Pile, in *Proceedings of IPAC2015* (2015) TUPWI047.
 - [4] T. Uemura, W. Fischer, *et al.*, “ μ SR at BNL,” (2014), summary talk at Transformative Beamline Workshop, BNL, ”<https://indico.bnl.gov/contributionListDisplay.py?confId=719>”.
 - [5] T. Roberts, *G4beamline User’s Guide 2.12*, Tech. Rep. (Muons Inc., 2012).
 - [6] R. Chehab *et al.*, *IEEE Trans. on Nucl. Sci.* **NS-30**, 2850 (1983).
 - [7] A. Bungau, R. Cywinski, C. Bungau, P. King, and J. S. Lord, *Phys.Rev.ST Accel.Beams* **17**, 034701 (2014).
 - [8] D. Cochran, P. Dean, P. Gram, E. Knapp, E. Martin, *et al.*, *Phys.Rev.* **D6**, 3085 (1972).
 - [9] J. R. Haines and C. C. Tsai, *Graphite Sublimation Tests for the Muon Collider/Neutrino Factory Target Development Program*, Tech. Rep. ORNL/TM-2002/27 (ORNL, 2002).
 - [10] P. Thieberger, *Upper Limits for Sublimation Losses from Hot Carbon Targets in Vacuum and Gasses*, Tech. Rep. MUC-0186 (BNL, 2000).
 - [11] K. Olive *et al.* (Particle Data Group), *Chin.Phys.* **C38**, 090001 (2014).
 - [12] N. Cartiglia, “Ultra-Fast Silicon Detector,” (2015), ”SLAC seminar 7, Jan. 2015”, ”www-group.slac.stanford.edu/ais/publicDocs/presentation209.pdf”.
 - [13] Y. Kuno, “High-intensity muon beams in Osaka,” (2014), invited talk at Transformative Beamline Workshop, BNL, ”<https://indico.bnl.gov/contributionListDisplay.py?confId=719>”.
 - [14] S. Cook *et al.*, *Journal of Physics: Conf. Ser.* **408**, 012079 (2013).

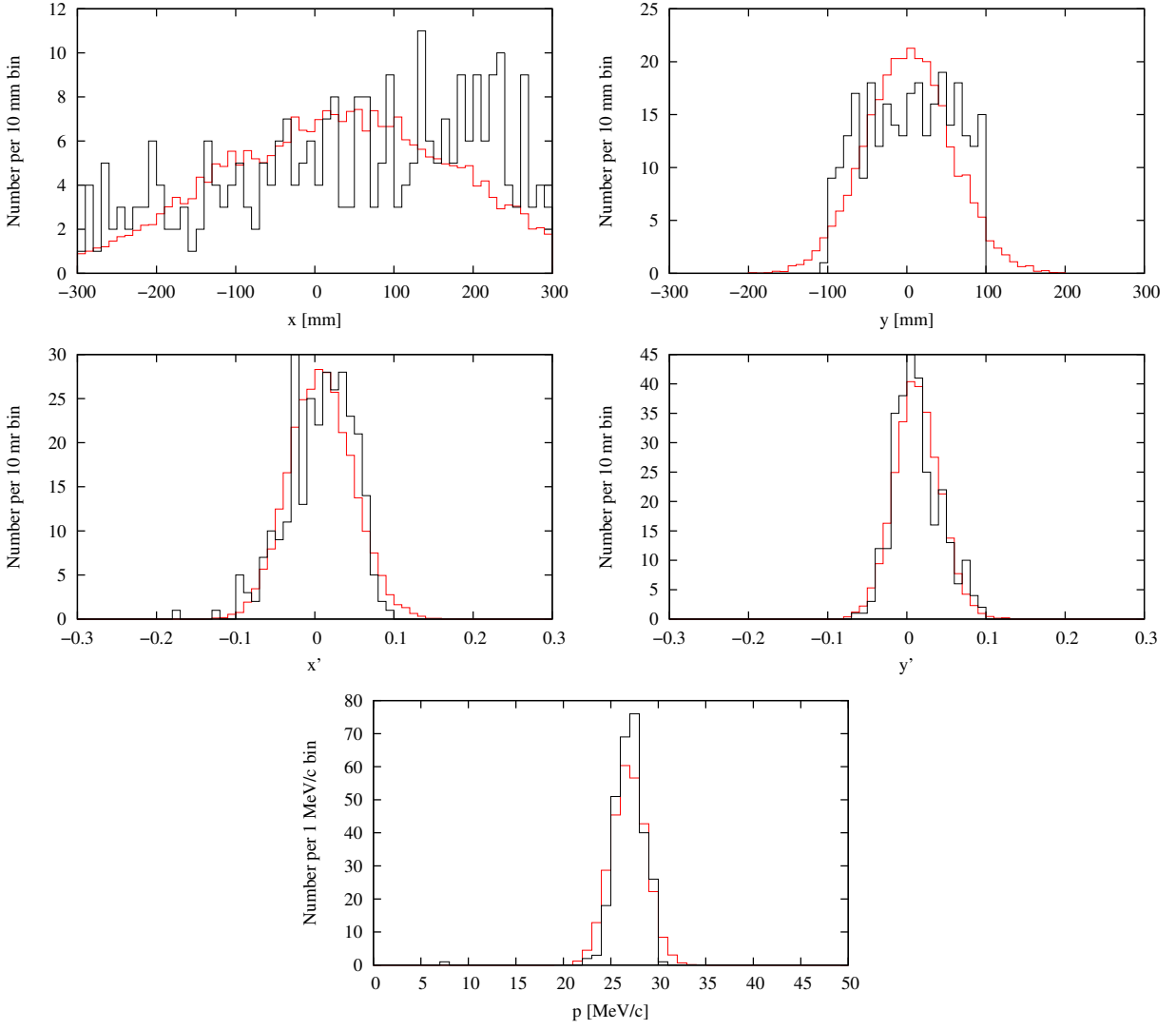


FIG. 39. Comparison of phase space projections for distribution at det18 just downstream of the 2nd separator. The black data contains 287 μ^+ at det18 from tracking muons 10^8 protons on the target with $\sigma_v^* = 5$ mm. The red histograms are divided by 34.8 and show the distributions from the 10,000 μ^+ generated by the 6-d phase space generator.

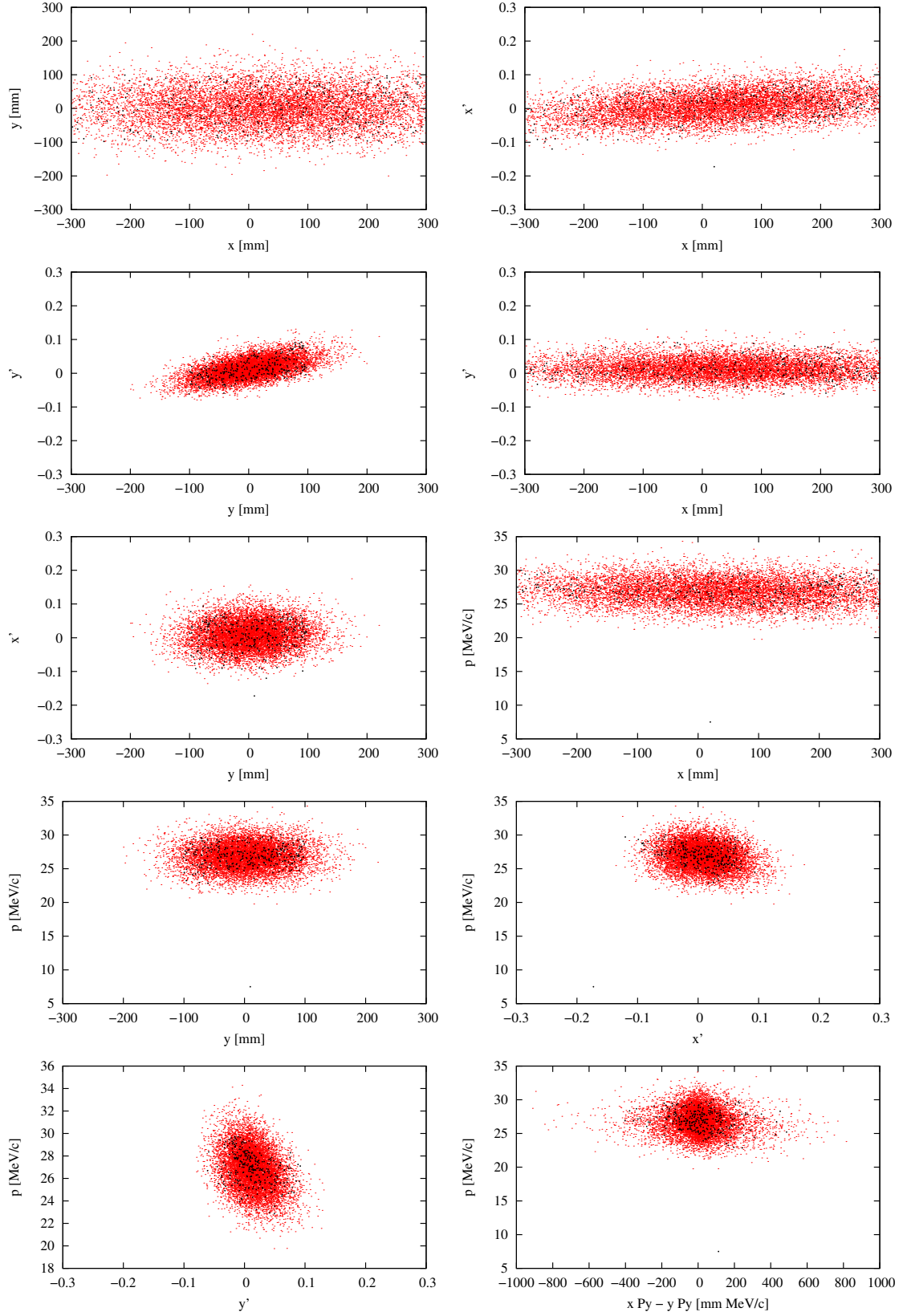


FIG. 40. Comparison of the phase space correlations at det18 of the 287 μ^+ in black from tracking and the 10,000 μ^+ from the 6-d generator in red.